Journal of Materials Chemistry B

ROYAL SOCIETY OF CHEMISTRY

PAPER

View Article Online
View Journal

Cite this: DOI: 10.1039/d6tb00211k

SAXS study of electric field-induced microstructural evolution in a polyaniline-based conductive hydrogel

Liu Tang, *[a] Yining Sun, [a] Robert F. Schmidt, [a] Clement Blanchet[b] and Michael Gradzielski *[a]

The behavior of conductive polymer networks under applied electric field plays a critical role in the electro-driven drug release of conductive hydrogels. This study investigates a novel conductive hydrogel composed of quaternized chitosan grafted with polyaniline (QCSPA) crosslinked with polyvinyl alcohol (PVA) and borate (BA), focusing on its structural evolution under varying electric fields. Small-angle X-ray scattering (SAXS), analyzed with the correlation length model and Gaussian spherical domain (GSD) fitting, was used to quantitatively characterize the multiscale structure of the hydrogel network. Under natural swelling, the spacing between network chains gradually increased, accompanied by a slow expansion of domain radius and correlation length, while maintaining a surface fractal, random coil-like structure. At 3 V, electric field-induced chain aggregation and swelling-driven expansion resulted in an initial slight contraction of domains followed by gradual expansion, reflecting a transition from mass to surface fractal behavior. Under a 5 V high electric field, chain aggregation intensified, leading to rapid formation of larger, denser domains and an accelerated shift to surface fractal structures. The aggregation and densification of spherical domains reduced the correlation length and accelerated polymer chain breakage and network erosion. Consequently, electric field stimulation drives a transformation of the hydrogel network from a microscopically disordered, loose state to an ordered, more densely packed multiscale structure, accompanied by accelerated macroscopic degradation and a significant reduction in mechanical performance.

Received 27th January 2026,
Accepted 23rd March 2026

DOI: 10.1039/d6tb00211k

rsc.li/materials-b

1. Introduction

Hydrogels are three-dimensional polymeric materials containing large amounts of water with crosslinked network structures.[1] This unique structure imparts excellent water absorption capacity while maintaining structural integrity and mechanical stability.[2] Naturally the main polymers in hydrogels must be of hydrophilic nature and the cross-linking can be of physical or chemical nature, or a mixture thereof. A particular subclass of them are stimuli-responsive hydrogels that can alter their microscopic conformations in response to external stimuli such as temperature, pH, ionic strength, light, or electric fields, thereby adaptively adjusting and modifying their macroscopic properties, including rheological, electrical, optical, thermal behaviour,[3,4] and shape modifications.[5]

In recent years, especially conductive hydrogels have attracted widespread attention in sensoring and biomedical applications due to their ability to combine electrical conductivity with the flexible mechanical properties of hydrogels and thereby also to be able to interface with biological tissue.[6,7] Conductive hydrogels are typically formed by integrating natural or synthetic polymers with conductive materials. These conductive materials include conductive polymers (such as polyaniline (PANI), polypyrrole (PPY), or polythiophene (PTH)), conductive carbon-based materials (such as carbon nanotubes (CNTs), graphene, and graphene oxide (GO)), metallic nanoparticles (such as Au and Ag), and conductive ionic compounds (such as Fe^{3+} and Al^{3+}).[8,9] Electrically responsive conductive hydrogels have been widely advanced in the development of smart drug delivery systems due to their unique electro-responsiveness, enabling precise control over drug release rates and timing by modulating the applied voltage or current.[10] Moreover, by appropriate choice of their components they can be made compatible to biological tissue, thereby opening up promising potential to be employed in a larger number of potential applications, for instance in chronic disease management and wearable healthcare devices.[11]

[a] Stranski-Laboratorium für Physikalische und Theoretische Chemie, Institut für Chemie, Technische Universität Berlin, D-10623 Berlin, Germany. E-mail: tangliu.tub@gmail.com, michael.gradzielski@tu-berlin.de
[b] European Molecular Biology Laboratory (EMBL), Hamburg Outstation, DESY, Hamburg, 22607, Germany

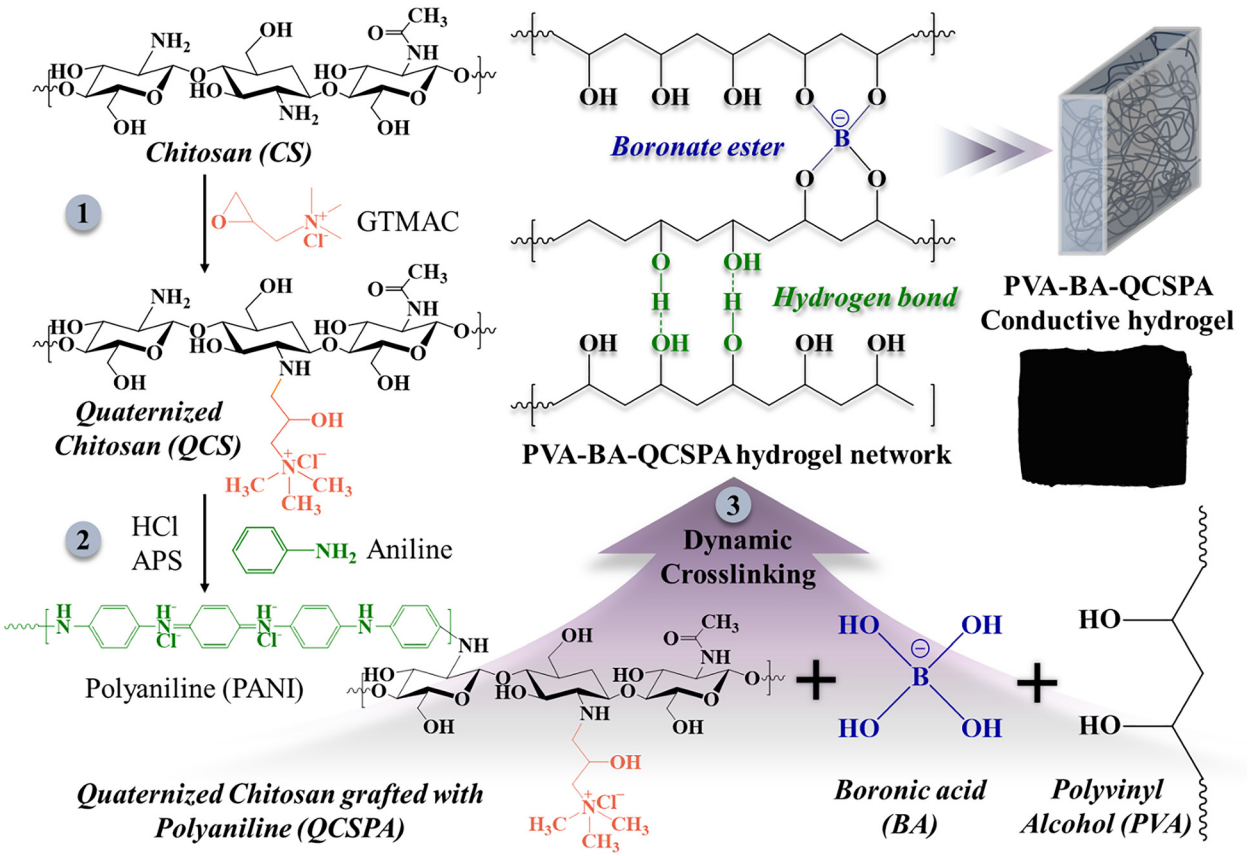

Fig. 1 Schematic route of preparation of the PVA-BA-QCSPA conductive hydrogel.

Polyaniline (PANI) is a conductive polymer renowned for its outstanding electrochemical activity, stability, and good biocompatibility (although less than polypyrrole).[12,13] Its electrical conductivity depends strongly on its oxidation state and degree of protonation.[14] In its half-oxidized state (the conductive form), alternating oxidized and reduced units along the PANI chain enable electron transport through a π–π conjugated system, facilitating charge mobility along the polymer backbone (structure of PANI is shown in Fig. 1).[15] The incorporation of PANI not only significantly enhances the overall conductivity of the hydrogel, enabling rapid and efficient responses to external electric field changes, but also improves the hydrogel's mechanical stability and durability.[16] Due to its unique chemical structure, PANI can be readily grafted onto chitosan, thereby imparting enhanced water solubility and antioxidant properties.[17] Quaternized chitosan grafted with polyaniline copolymers have been reported to exhibit superior antibacterial activity and improved cell compatibility compared to pure quaternized chitosan.[18]

Small-angle X-ray scattering (SAXS) is a powerful analytical technique to characterize the internal structure of materials on the nanoscale to microscale, including pore size, particle morphology, and their distribution.[19–21] Polymer chains can adopt a variety of architectures—such as linear, star-branched, dendritic, bottlebrush, or cyclic—each influencing the properties of the resulting polymer composites.[22] Therefore, SAXS plays an important role in hydrogel research, as it provides an *in situ* method for observing and analysing the three-dimensional network structure, pore architecture, crosslinking density, interactions between polymer segments, and dynamic behaviour of hydrogels.[23–25] The technique can be applied directly to hydrated bulk samples without drying, enabling the acquisition of averaged structural information under application-relevant conditions and allowing for the determination of the relative size and conformation of individual components.[26,27]

In a previous study, we synthesized a conductive polymer QCSPA (quaternized chitosan, QCS, modified with polyaniline, PA), which was subsequently crosslinked with poly (vinyl alcohol) (PVA) and boronic acid (BA) to form a conductive hydrogel loaded with insulin. This PVA-BA-QCSPA conductive hydrogel exhibited excellent conductivity and enabled modulation of insulin release rates in response to external electric fields. However, the microstructural evolution of the hydrogel under electric stimulus and its impact on drug release remained unexplored. Conventional microscopy can only observe the freeze-dried state of the samples, but freeze-drying alters the microstructure of hydrogel, such as polymer chain aggregation and conformational behaviour, and cannot provide accurate information on chain size or conformation.[28,29] This limitation is particularly critical when electric fields are applied, as any field-induced microstructural changes are likely eliminated

during the drying process. In contrast, SAXS is well-suited for *in situ* determining the size, shape, concentration, and conformation of polymer chains and assemblies in the 10–100 nm range.[25] Therefore, we employed SAXS to perform non-destructive, *in situ* analysis of this multicomponent conductive hydrogel system.

Accordingly, we employed SAXS in this study to determine the changes in the polymer network structure of the PVA-BA-QCSPA conductive hydrogel for applying electric fields for different durations of time. In this work, we focus on the mechanism and evolution of the hydrogel microstructure under electrical stimulation using a representative formulation. From this investigation we can deduce how the structure of the hydrogel changes during the swelling process in the presence of an applied electric field compared to its absence. This is a central information, for understanding the performance of these electric field responsive hydrogel materials in electro-driven drug release.

2. Materials and methods

2.1 Materials

Chitosan (low molecular weight, 50 000–190 000 Da), acetic acid (AcOH, ≥99.0%), acetone (≥90%), agarose, ammonium persulfate (APS, ≥98.0%), aniline (99%), boric acid (BA, ≥99.5%), glycidyltrimethylammonium chloride (GTMAC, ≥90%), *N*-methyl-2-pyrrolidone (NMP), polyvinyl alcohol (PVA, degree of alcoholysis = 98–99% mol/mol) and phosphate buffered saline (PBS, pH = 7.4, 0.01 M) were obtained from Sigma-Aldrich. Dialysis bags with cut-off 14 000 Da were purchased from Carl Roth GmbH. Ultrapure water (Milli-Q) with a resistivity of 18.2 MΩ cm at 25 °C was used as solvent throughout the study. All chemicals were analytical grade and used as received without further purification.

2.2 Synthesis and preparation of PVA-BA-QCSPA conductive hydrogel

The synthesis and preparation process of the PVA-BA-QCSPA conductive hydrogel is shown in Fig. 1. At first, the QCSPA conducting polymer was synthesized by steps 1 and 2. Cho's method was used to perform quaternization modification of chitosan.[30] 5 g of chitosan were dispersed in 200 mL of water with 1 mL of AcOH and the mixture stirred at 300 rpm for 30 minutes. Subsequently, 9.2 mL of GTMAC was added dropwise and the reaction temperature was maintained at 65 °C for 18 hours. After the reaction, the mixture was centrifuged at 4000 rpm for 20 minutes to remove any undissolved precipitates. This supernatant was then treated with an excess of acetone to extract the synthesized polymer. The polymer was redissolved in water, dialyzed for five days to remove residual solvent and low molecular weight impurities, and lyophilized to obtain QCS. Subsequently, QCSPA was prepared by using a 7% feed ratio (mass ratio of aniline monomer to QCS) with referring to Zhao's method.[18] 500 mg of QCS was dissolved in 60 mL of 0.1 M HCl solution and cooled to 4 °C in an ice bath. 35 μL of aniline was then added and stirred for 1 h. Following this, 84 mg of APS was added and stirred for 1 h. The ice bath was removed, and stirring continued at room temperature for 24 hours. The pH was adjusted to neutral, and excess acetone was added until precipitation ceased. The precipitate was washed with NMP to eliminate any unreacted aniline monomer or unbound PANI and redissolved in water. The amount of free aniline or PANI was quantified using UV-Vis spectroscopy, and the grafting yield (the aniline amount attached on the QCS) was 99.3%. After five days of dialysis, the QCSPA was obtained by lyophilization.

Fourier transform infrared spectroscopy (FTIR) analysis of the synthesized polymers was performed using an IR spectrometer (ID7, Thermo Fisher Scientific, USA) in an ATR mode. The FTIR spectra of lyophilized QCS and QCSPA are shown in Fig. S1. Compared with QCS, QCSPA displays the signal of GTMAC at 1475 cm^{-1}, along with the PANI at 1572 cm^{-1} (quinine diimine ring stretching) and 1490 cm^{-1} (benzenoid diamine ring stretching).[31] Accordingly, QCSPA exhibits characteristic PANI-related bands in the 1500–1600 cm^{-1} region (ring vibrations), supporting that PANI was successfully grafted onto the QCS backbone *via* a C–N bond. Furthermore, the QCS amine-related band at 1560 cm^{-1} (N–H bending of amide-II) is weakened, indicating a changed chemical environment of the amino groups consistent with C–N grafting.[32]

For the preparation of PVA-BA-QCSPA hydrogel, first a 10% QCSPA solution was prepared by mixing with 1 M HCl and water to achieve a molar ratio of *M*(quinoid units): *M*(HCl) of 2 : 1.[18] PVA powder was dissolved in water and heated to 90 °C until dissolution was complete and homogeneous. Then, we took 1.2 mL 10% QCSPA solution, 2 mL 30% PVA solution and 0.425 mL of water, and stirred continuously for 30 minutes until thoroughly mixed. Then 0.375 mL 16% neutral BA solution was added for crosslinking under sufficient stirring until the hydrogel was formed. The crosslinked hydrogel was transferred into a graduated syringe mould (6 mL), and air was expelled by compression. It was then placed in a refrigerator overnight to ensure overall equilibrium and to homogenize the hydrogel. Finally, the resulting conductive hydrogel of 15%PVA-1.5%BA-3%QCSPA was prepared as shown in Fig. 1. The PVA-BA-QCSPA hydrogel is primarily constructed *via* dynamic boronate ester crosslinks, while electrostatic interactions introduced by the quaternary ammonium groups, together with hydrogen bonding, also participate in regulating the network. PVA likely forms the primary network backbone and provides diol sites for reversible boronate crosslinking with BA, but it should be noted that also the chitosan OH-groups will become crosslinked to a certain extent here. The ratio of PVA/BA directly influences the crosslink density and basic mesh size. QCS serves as the backbone carrying the conductive polymer, introducing quaternary ammonium groups and PANI segments, thereby increasing hydrophilicity and ionic transport within the network.

Following the preparation of the PVA-BA-QCSPA conductive hydrogel, electrical stimulation at varying voltages was applied, as shown in Fig. 2. A 0.4 mL hydrogel sample was wrapped around the positive carbon electrode and immersed in 10 mL of

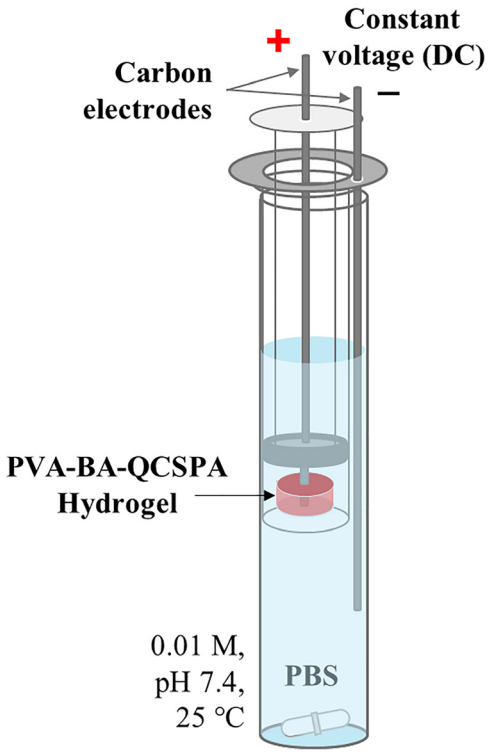

Fig. 2 Schematic of DC constant voltage stimulation in the PVA-BA-QCSPA conductive hydrogel.

PBS (0.01 M, pH 7.4, 25 °C), while the negative carbon electrode (a carbon rod with a diameter of 2 mm) was directly immersed in the same PBS solution. Both carbon electrodes were connected to a DC constant voltage source to provide a stable external electric field. At 25 °C, hydrogel samples were exposed to DC constant voltages of 0 V, 3 V, and 5 V for varying durations (0.5, 1, 2, 4, and 24 hours), which corresponds to experimental field strengths ($E = V/d$) of approximately 0, 3 and 5 V cm^{-1}. After stimulation, the hydrogel samples were gently blotted to remove surface moisture and stored in sealed centrifuge tubes for subsequent rheology and SAXS measurements.

2.3 Rheology

The rheological behaviours of the hydrogels were tested in strain mode using the parallel plate measurement system of the rheometer MCR502 (Anton Paar, Austria). 250 μL of equilibrated hydrogel was placed between the plate-plate measuring system with 25 mm diameter and final gap of 0.5 mm. The frequency sweep was performed over the range of 0.1–100 rad s^{-1} at a strain of 0.1%, which is within the linear viscoelastic region as shown by strain sweeps. The strain sweep was tested from 0.1% to 20% at a frequency of 1 Hz. An alternate strain sweep was conducted to observe the recovery properties of the gel using cyclic switching from small strain (1%) to large strain (100%). Each strain level was maintained for a duration of 150 s and the storage modulus G' and loss modulus G'' were recorded over the time. All measurements were performed at 25 °C.

2.4 Small-angle X-ray scattering (SAXS)

SAXS, as an elastic scattering technique, provides information at different length scales by measuring scattering intensity at various scattering angles θ.[33] Fig. 3 illustrates a standard SAXS setup, where a highly collimated and monochromatic X-ray beam with wavelength λ passes through the sample. The intensity of the X-ray that is elastically scattered is captured by a 2D detector and the scattering angle θ is inversely related to the size of the scattering object.[34] For fully elastic scattering (no energy transfer) the magnitudes of incident k_i and scattered k_s wavevector are equal, and the magnitude of the vector q can be calculated by:

$$q = |\vec{q}| = \frac{4\pi}{\lambda}\sin\left(\frac{\theta}{2}\right) \quad (1)$$

The normal size scale in a scattering experiment is determined by the range of $2\pi/q$ covered, as the q value is inversely related to the size of the structures being probed.

One day prior to SAXS testing, the PVA-BA-QCSPA conductive hydrogel was subjected to electrical stimulation under different voltages and for different lengths of time to prepare electrically stimulated samples of different degrees, as shown in Fig. 2. SAXS measurements were conducted at the P12 beamline of the European Molecular Biology Laboratory (EMBL) located on the PETRAIII storage ring (Hamburg, Germany). For the SAXS measurement, all hydrogel samples were loaded for measurement in a gel holder equipped with round mica windows with an optical path length of 1 mm. The X-ray incident wavelength was 0.124 nm, with a beam size of 100 × 200 μm and a beam

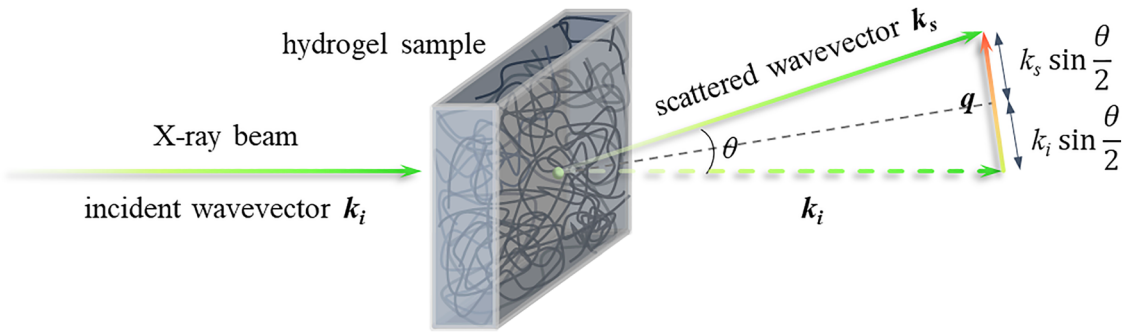

Fig. 3 Schematic of SAXS measurement principle.

flux of 10^{12} photons per s. Scattered photons were collected on a Pilatus 6M detector (Dectris, Switzerland) with a sample-to-detector distance of 6 m, covering a q-range of 0.02–4.5 nm^{-1}. All measurements were performed at 25 °C. For each measurement, 10 frames were collected and checked for radiation damage before averaging. Background scattering from H_2O and the sample holder (empty-window background) was first subtracted using the ATSAS software package. All datasets were normalised according to beam intensity. The resulting data were further converted to an absolute scale using a previously validated method.[21] To calculate the scattering intensity in the absolute scale, the known scattering of water ($I_{0,abs}$(water) = 1.633×10^{-2} cm^{-1}, at 25 °C), was used. By dividing the relative intensity of the samples with the experimental constant scattering of water and then multiplying by the absolute scattering of water one obtains the intensity of the samples in absolute scale.

3. Results and discussion

3.1 Rheological behaviour of hydrogels

Rheological tests were conducted on PVA-BA-QCSPA hydrogel after electrical stimulation at different voltages (Fig. 2) to evaluate how their mechanical behaviour changed due to the variation. The strain sweeps shown in Fig. 4 were conducted to determine the linear viscoelastic (LVE) region at a fixed frequency of 1 Hz. The LVE extended well above 10% strain and the larger the LVE regime, the more the material is elastically deformable. In all cases, G' is significantly larger than G'', confirming primarily elastic behaviour as expected for hydrogels. The average values of storage modulus G' and loss modulus G'' in this region were used to characterize the state of the hydrogel after different voltage treatments. As shown in Fig. 4a, when the PVA-BA-QCSPA hydrogel was swollen in PBS without any voltage applied, both G' and G'' decreased over time. After 24 hours, not only had the modulus significantly declined, but the gap between G' and G'' also narrowed substantially, indicating a relatively greater loss in elastic behaviour. This suggests that with increasing swelling time, the gradual hydrolysis of borate ester bonds and hydrogen bonds led to dissociation and loosening of the hydrogel network, resulting in reduced crosslinking density, decreased mechanical strength, and a softer hydrogel state. Especially after 24 hours of swelling, G' and G'' became very close, indicating that the crosslinked network was highly weakened and approaching a near-dissociated state.

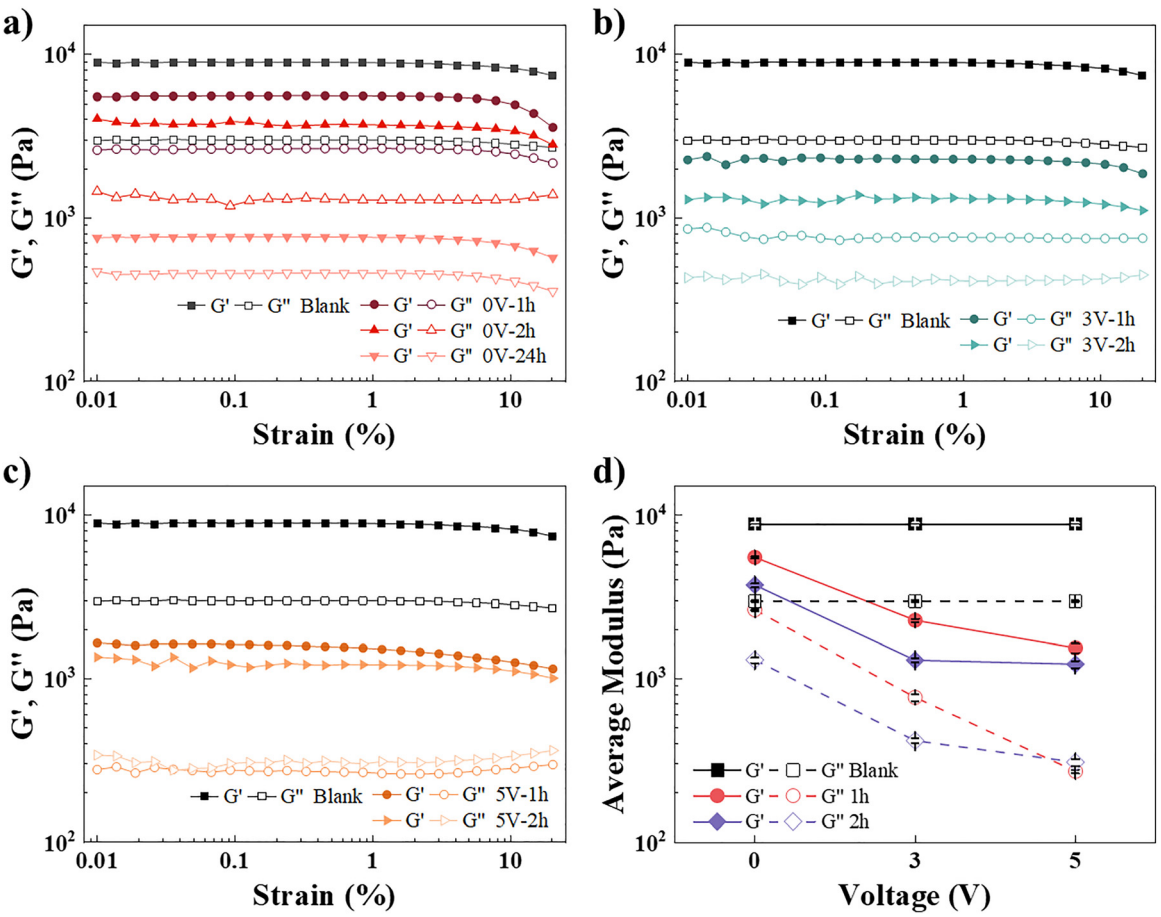

Fig. 4 Rheological behaviour of PVA-BA-QCSPA hydrogels after electrical stimulation at (a) 0 V, (b) 3 V, and (c) 5 V over time in strain sweep test. (d) Average G' and G'' of PVA-BA-QCSPA hydrogels after electrical stimulation at different voltages for different times.

When a constant voltage of 3 V was applied for 1 h and 2 h, as shown in Fig. 4b, the trends of G' and G'' were similar to those observed during the swelling process in Fig. 4a, both decreasing over time, but the extent of the decrease was significantly larger under electrical stimulation. After just 1 hour under 3 V, the decreases in G' and G'' were greater than those observed at 2 hours without voltage. Notably, the reduction in G'' was more pronounced, reaching a level comparable to 24 hours of natural swelling after just 2 hours under 3 V. This indicates that the applied electric field can accelerate the reduction of both the elastic and viscous behaviour of the hydrogel. Mechanistically, the DC field promotes ion migration and electroosmosis in PBS, accelerating water absorption and plasticization in the early stage, while the field-induced redistribution of ions and local electrochemical environment could facilitate dissociation of the dynamic boronate crosslinks and weaken hydrogen-bonding interactions, thereby leading to a faster reduction in the effective crosslink density and softening of the network. This effect becomes more pronounced at 5 V (Fig. 4c), where G' and G'' decrease further, demonstrating that stronger electrical stimulation accelerates network softening.

It is worth noting, however, that although G' and G'' showed a substantial decrease during the first hour at 5 V, the decrease rate slowed down in the second hour. This suggests that increased voltage reduces more rapidly elasticity and viscosity, thereby more effectively weakening the mechanical properties of the hydrogel. Comparison of the average modulus (average G' and G'' at high strain) of hydrogels after electrical stimulation at different voltages is shown in Fig. 4d. Obviously, at 5 V, the decline in G'' is more pronounced than that in G', and both G'' at 5 V – 1 h and 5 V – 2 h were much lower than the state of natural swelling for 24 h. This indicates that the viscous properties of the hydrogel were significantly diminished by voltage application, suggesting that the electric field may not simply accelerate the natural swelling and network dissociation process, but instead induce a certain degree of erosion and disruption to the hydrogel network structure, leading to dramatic changes in the rheological behaviour. Such field-induced erosion and dissolution would more markedly reduce dissipative contributions, providing a reasonable explanation for the more pronounced decrease in G'' at higher voltages. Therefore, comparing the hydrogel behaviour within the first and second hour, higher applied voltages led to greater reductions in both G' and G'', indicating that the extent of erosion and disruption to the hydrogel increased with the applied electric field strength.

The swelling curves of the hydrogel under different voltages, as shown in Fig. S2, exhibit similar trends. Without applied voltage, the mass of hydrogel gradually increased within 24 h, with the hydrolysis rate remaining lower than the swelling rate. When the 3 V voltage was applied, the swelling rate rose rapidly within the first hour but then slowed down, falling below that of the non-electrically stimulated sample, indicating that mass loss increased during swelling. Under 5 V, this trend became more pronounced—the swelling rate was fastest during the first hour but showed almost no change in the second hour, reaching a swelling–dissociation equilibrium, which is consistent with the slower decrease of G' and G'' from 1 h to 2 h at 5 V. Subsequently, mass loss exceeded water absorption, and the swelling ratio began to decline. The swelling curves indicate that the hydrogel undergoes rapid network weakening under the electric field, which enables fast initial swelling; however, the subsequent collapse and dissociation of the network lead to increased mass loss, causing the swelling ratio to decelerate rapidly and even decline. This behaviour also corresponds to the greater reduction in average modulus observed in the rheological analysis at higher voltages. Moreover, the difference for 3 V and 5 V becomes noticeably smaller at 2 h (Fig. 4d), this may suggest a potential time-dependent ''early saturation'' behaviour under the stronger field.

From the thermodynamic perspective of hydrogel swelling, the overall behaviour can be summarized by a competition among polymer–solvent mixing contributions, elastic network forces (set by the effective crosslink density), and ionic osmotic pressure. In the present system, the PVA-BA boronate crosslinks govern the elastic contribution, whereas QCS and protonated PANI introduce fixed charges and thus ionic/osmotic contributions. Under a DC field in PBS, ion migration and electroosmotic transport can modify the ion concentration, thereby modulating the ionic/osmotic driving force for water uptake. Meanwhile, electrical stimulation can accelerate loss of effective network connectivity *via* dynamic boronate bond dissociation and weakened noncovalent interactions, and at higher voltage and longer times can promote erosion-like mass loss. Consequently, at 5 V the hydrogel quickly reaches a swelling–dissociation balance and then shows increased mass loss, implying that the electrical field-induced disruption becomes limited likely by the transport constraints of the remaining network. These effects lead to diminishing returns in modulus reduction at higher voltages.

3.2 SAXS characterization and analysis of hydrogels

3.2.1 SAXS intensity curves – Kratky plot. To investigate the electric field-induced microstructural changes in PVA-BA-QCSPA hydrogels and analyse their drug release mechanisms, we performed SAXS characterization on hydrogels subjected to different durations of exposure at 0 V, 3 V, and 5 V. The resulting scattering curves are given in Fig. S3 as normal intensity plots.

The Kratky plot, *i.e.* $I(q) \times q^2$ *versus* q, is a widely used visualization method in SAXS data analysis.[35] This plot enhances the visibility of structural features across multiple length scales, enabling a more intuitive distinction of compact globular structures, random coils, and rigid rod-like conformations in polymers, proteins, hydrogels, and other soft matter systems.[26,36] Specifically, the shape, position, and high-q decay behaviour in the Kratky plot reflect the compactness of the material.[37] For instance, the scattering intensity of flexible Gaussian chains decays at a rate of approximately q^{-2} or more slowly. As a result, the Kratky plot of an ideal Gaussian chain increases monotonically with q and approaches a plateau at high-q.[38] In contrast, the scattering intensity of compact globular

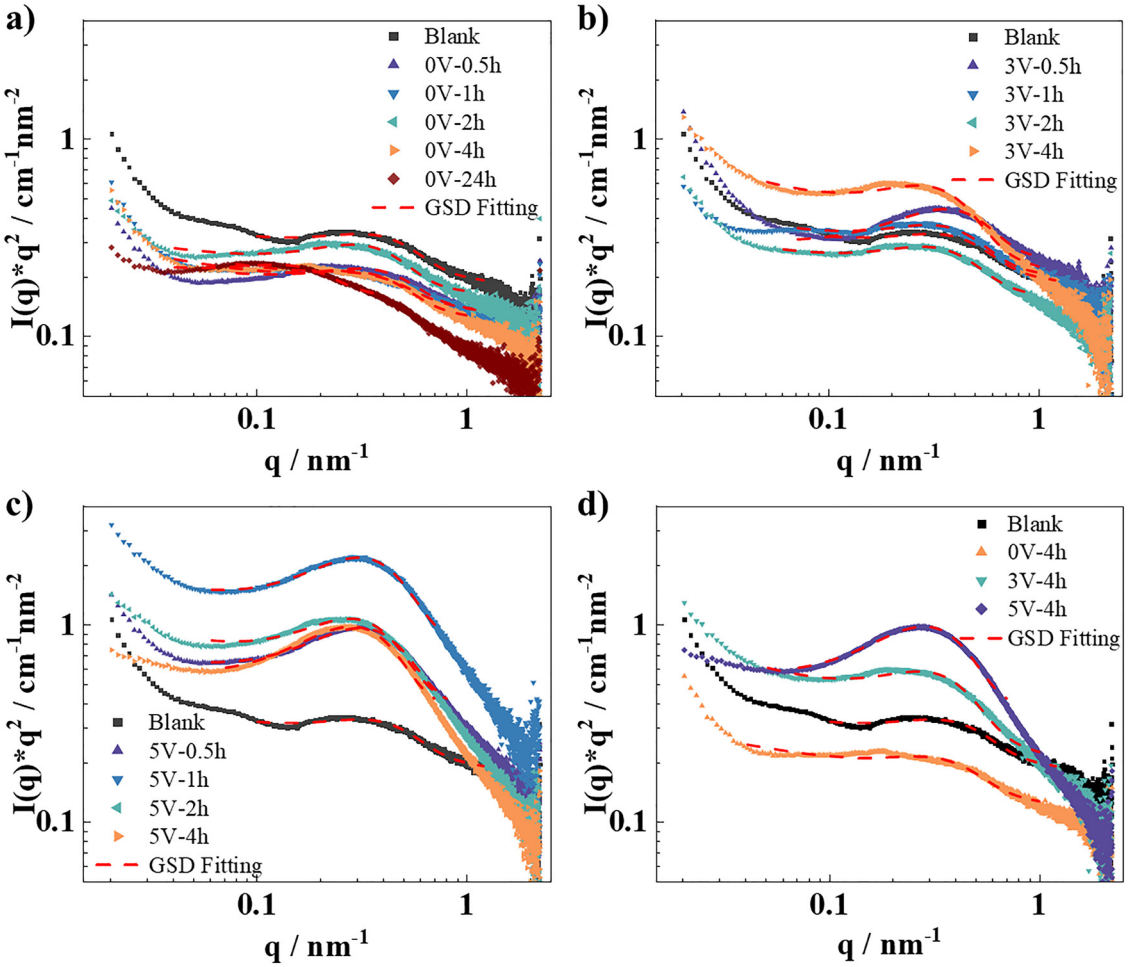

Fig. 5 Kratky plots from SAXS curves of the PVA-BA-QCSPA hydrogel with the application of (a) 0 V, (b) 3 V, and (c) 5 V. (d) Comparison of the PVA-BA-QCSPA hydrogel at different voltages for 4 h. The red dashed curves represent the Gaussian spherical domain (GSD) fitting curves by eqn (4).

domains decays at higher q approximately as q^{-4}, leading to a bell-shaped Kratky plot with a pronounced peak, followed by a decline of q^{-2} at high-q.[39,40] Prior to plotting the Kratky, the background (Bkg) in the high-q region ($q > 0.8$ nm^{-1}) was first subtracted from each scattering curve using eqn (2). The resulting Kratky plots is presented in Fig. 5.

As shown in Fig. 5a, when the hydrogel swells naturally in PBS, the original hydrogel exhibits a broad peak around 0.25 nm^{-1} followed by a slow decline in the Kratky plot. This indicates that the hydrogel, in the absence of electrical stimulation, exhibits a distance distribution of scattering elements like in a flexible random coil structure, characterized by loosely arranged network segments and no compacted aggregates. From 0.5 to 4 hours of swelling, the Kratky intensity reduces and the peak moves to lower q values and broadens, indicating that the hydrogel structure gradually relaxes and slightly swells over time, thereby enhancing the flexibility of polymer chains. Their dilution explains the reduction of scattering intensity. After 24 hours of swelling, the curve shows a further leftward shift, accompanied by a pronounced decay in the high-q region. This indicates that in the swelling process the network relaxes and the spacing between characteristic polymer domains increases and this is a rather slow process. Simultaneously, the local arrangement of polymer segments tends to a more compacted structure. This phenomenon is likely related to the partially rigid and conjugated structure of PANI, which promotes π–π stacking and interchain attractions. Thus, during hydrogel swelling, PANI chains gain the freedom to aggregate into nanoclusters, leading to a synergistic evolution characterized by local densification and overall network expansion.

Upon application of 3 V, as shown in Fig. 5b, one observes an increased Kratky peak intensity that shifts to higher q values at 0.5 h, indicating rapid aggregation and contraction of hydrogel polymer chains under the electric field. From 0.5 to 4 h the Kratky peak progressively shifts back to lower q values but retaining an increased intensity. This reflects that the local domains expand much less and contain more polymer. Meanwhile, the electric field may induce partial orientation or local rearrangement of charged chain segments or PANI components, enhancing local density fluctuations and aggregation. After 4 hours of 3 V stimulation in PBS, the Kratky plot shows a significant increase at low-q and rapid decay at high-q,

suggesting enhanced large-scale density fluctuations within the network and locally the structure becomes more compact. This behaviour likely results from suppressed swelling due to the electric field and a rearrangement of the conductive component PANI which leads to localized densification. Consequently, the electric field-induced chain aggregation counterbalances the swelling-induced expansion. This "macroscopically loose–microscopically dense" multiscale structural evolution represents the opposite effects of swelling and electric stimulation.

For applying 5 V (Fig. 5c), the Kratky plot displays a much more marked peak with initially much increasing intensity that becomes reduced again after about 1 h. The peak shifts only slightly toward higher q values, but now a steep decay is observed in the high-q region. This indicates rapid aggregation of hydrogel polymer chains and the formation of highly dense domains under the strong electric field, followed by subsequent swelling for longer times. In contrast to the situation at 3 V the application of 5 V induces enhanced orientation, compaction and aggregation of charged PANI chains, thereby accelerating the electric field-driven structural evolution. Interestingly the Kratky intensity at low q becomes much reduced for longer times, indicating a higher degree of order on a larger size scale of >100 nm.

A comparison of the Kratky plots after 4 hours under different voltages, as shown in Fig. 5d, clearly illustrates the impact of the electric field. Without applied electric field, the overall curve shifts downward and the peak moves to lower q, indicating that the structures become larger but also much more dilute by polymer. With increasing voltage, the hydrogel network undergoes a structural evolution from a loose to a moderately contracted and finally a highly densified state. Initially, the hydrogel exhibits a flexible random coil-like structure. Under 3 V, chain segment rearrangement and moderate aggregation induced by the electric field cause an increase in peak value and contraction of peak shape. At 5 V, a pronounced Kratky intensity increases and a steep decay in the high-q region are observed, signifying the strongest network contraction and aggregation, driven by the higher voltage. The comparison comprehensively reveals the multiscale structural evolution of the conductive hydrogel under electric stimulation and its suppression of the normal hydrogel swelling.

3.2.2 Correlation length model. Scattering experiments give information about density fluctuations, such as the average mesh size in polymer networks or the interfacial width in two-phase systems.[33,34] For a quantitative analysis of the scattering data, the correlation length model (eqn (2)), as described by Hammouda *et al.*[41] was employed. It is given by:

$$I(q) = \frac{A}{q^n} + \frac{C}{1 + (q\xi)^m} + Bkg \qquad (2)$$

where q is the modulus of the scattering vector, and Bkg represents the incoherent background scattering. The first term

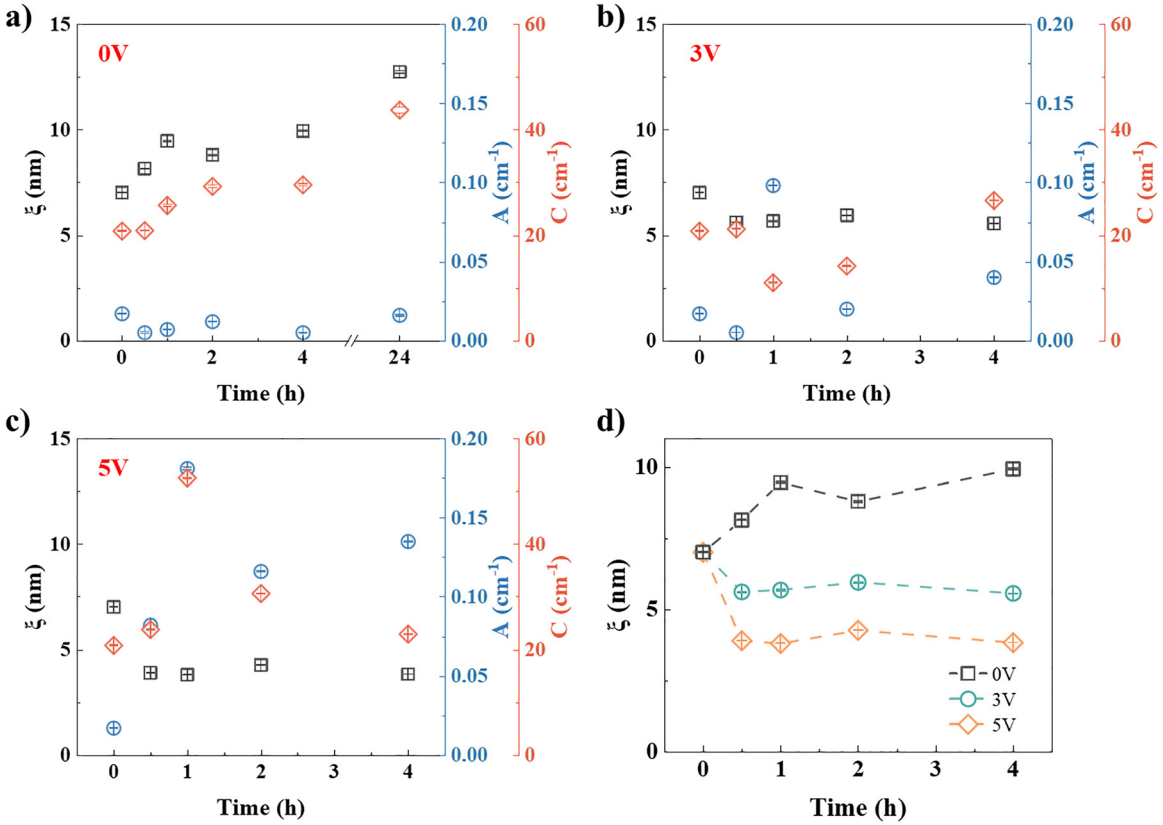

Fig. 6 Fitting parameters (ξ, A, and C) obtained from the correlation length model of PVA-BA-QCSPA hydrogels with the application of (a) 0 V, (b) 3 V, and (c) 5 V. (d) Comparison of ξ at different voltages over time.

describes scattering at low q from clusters with n as corresponding Porod exponent[42] that characterizes the fractal structure of the hydrogel network. The second term describes the local structure of the polymer chains with the correlation length ξ and the exponent m characterizing the interaction of the polymer chains with the solvent (for $m = 2$ becoming equal to the classical Ornstein–Zernike formula). ξ is the characteristic length scale associated with a mass fractal structure of the polymer network at smaller length scales[25,43] (and ξ could also be interpreted like an effective mesh size). A and C are fit parameters quantifying the relative contributions to the different structural features at the different length scales.

The scattering intensity $I(q)$ of the PVA-BA-QCSPA hydrogels were fitted over the entire q-range by the correlation length model (eqn (2)). The fitting parameters were determined by nonlinear least-squares fitting to minimize the difference between experimental and model intensities. The resulting fit parameters are given in Fig. 6 and 7 and the fitted curves are shown in Fig. S4–S6. A sketch representing this model is given in Fig. 8.

As shown in Fig. 6a, the correlation length ξ of the PVA-BA-QCSPA hydrogel during swelling in PBS only increases in the absence of an applied voltage. Initially the gel exhibited a correlation length of approximately 7 nm, which nearly doubled after 24 hours of swelling, with a similar increase of the intensity factor C. At the same time m (and also n, Fig. 7a) changed very little and stayed around 2.4, corresponding to a polymer network in a poor solvent. This suggests that during swelling in water, the local polymer domains expanded and the average distance between network segments increased, leading to an enlarged mesh size, while the internal statistical distribution of polymer chains within these domains remained essentially unchanged. In contrast, the power-law scaling factor A and exponent n remained nearly unchanged over the 24 h, indicating that the large-scale structure did not undergo substantial morphological transformation and the fractal or clustered organization of the network remained unchanged during swelling, consistent with an approximately affine swelling process.

Upon application of 3 V or 5 V to the conductive hydrogel, the correlation length ξ decreases with time (Fig. 6b and c), *i.e.* here not swelling related increase is observed. The trend of correlation length ξ over time under different voltages is directly compared in Fig. 6d and illustrates that, in contrast to

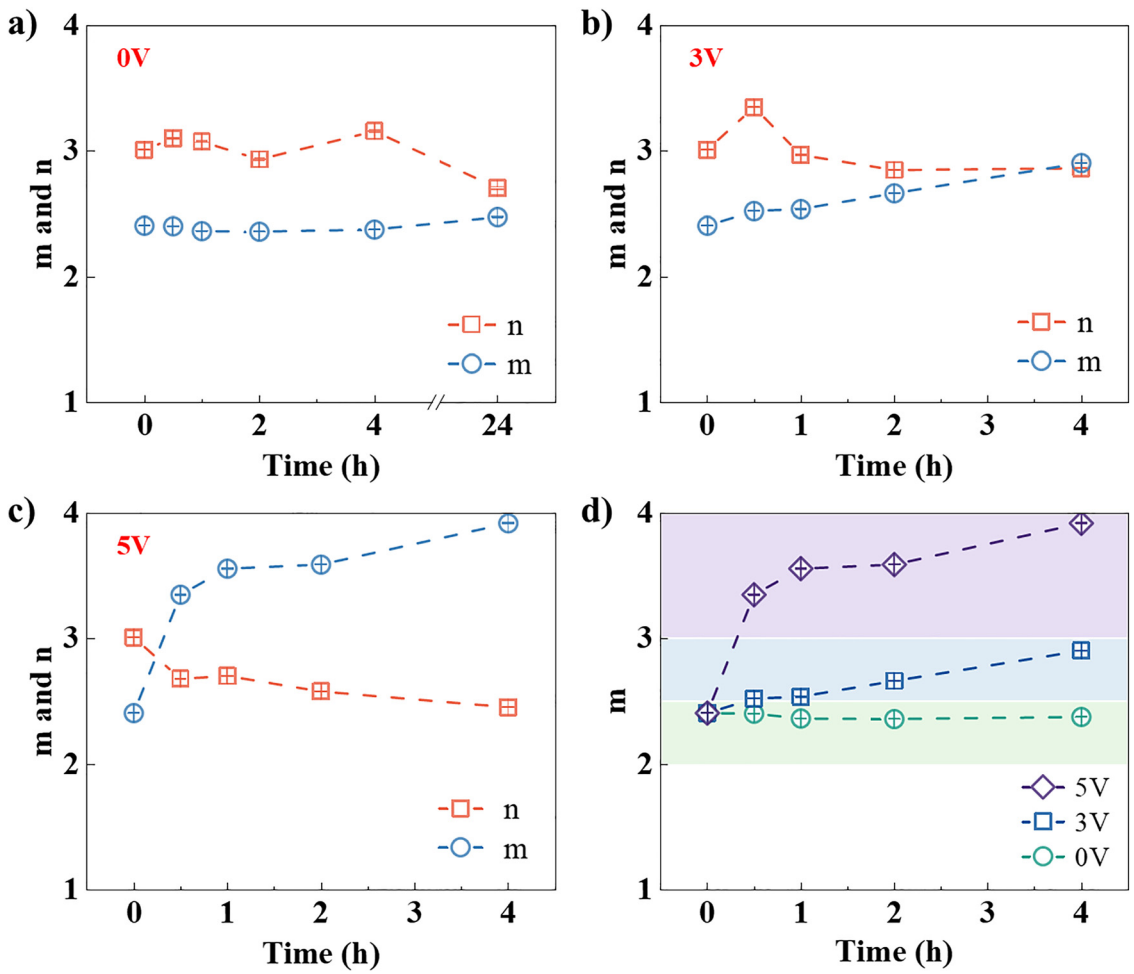

Fig. 7 Exponents (n and m) obtained from the correlation length model of the PVA-BA-QCSPA hydrogel with the application of (a) 0 V, (b) 3 V, and (c) 5 V. (d) Comparison of m at different voltages over time.

the case of no applied voltage, where ξ is substantially increasing, with the application of 3 V or 5 V, ξ is declining to 5.6 nm under 3 V and dropping even more significantly to ~3.8 nm under 5 V. This is consistent with the changes of the intensity factor C which is rather constant for 3 V, but for the case of 5 V C rises largely within 1 hour to a value of 52.5 cm^{-1} and then becomes reduced again to the initial value for longer times. This indicates that a stronger electric field rapidly induces domain growth and compaction of aggregated domains that reorganize again for longer times.

At the same time, the exponent m increases systematically over 4 hours from 2.4 to about 2.9 for 3 V and jumps rather quickly to 3.4 and rises further to about 3.9 for 5 V (Fig. 7b and c). For reference, m = 4 corresponds to particles with smooth surfaces, m = 3 indicates highly rough surfaces or collapsed polymer chains in poor solvents, m = 2 corresponds to scattering from Gaussian polymer chains or two-dimensional structures, and m = 1 would for instance be seen for scattering from stiff rods.[44] The variation trend of m under different voltages is highly characteristic, as shown in Fig. 7d. Correspondingly, after 4 hours under 3 V, the local polymer domains seem to have evolved toward structures resembling rough particles formed by collapsed polymer chains in a poor solvent, where this structural change occurs progressively under the application of the electric field. When the voltage was increased to 5 V, m exceeded 3 within just 1 hour and approached 4 after 4 hours. This transition indicates a shift from mass fractal to surface fractal behaviour, where the polymer chains within local domains became densely packed. Therefore, combining the observed changes of ξ and m, the evolution of the PVA-BA-QCSPA hydrogel network structure is depicted in Fig. 8. When no electric field is applied, the network exhibits swelling-driven expansion and loosening. Upon applying an electric field, it likely arises from the formation of highly ordered PANI chain arrangements and conductive pathways under the electric field, where higher voltage produce stronger field forces, thereby promoting tighter and more regular rearrangements of PANI segments within the network. This transition also corresponds to the reduced modulus in rheology and the accompanying decrease in effective network connectivity, leading to macroscopic mechanical weakening and erosion-like mass loss.

The changes in the power-law scaling factor A and n are then less systematic. The main finding is that at highest voltage of 5 V n is systematically decreasing (Fig. 7c), which indicates that the more compacted structures present there tend to be less organized in a disordered network but instead an overall ordering process has taken place.

It might be noted that one can convert the rheological moduli to an effective mesh size ξ_{rh} *via* the relation $G_0 = kT/\xi_{rh}^3$. Taking the values from Fig. 4 one would calculate a value of 7.8 nm for the initial gel and for the gels after 2 hours for the one without applied electric field and with 5 V 10.4 nm

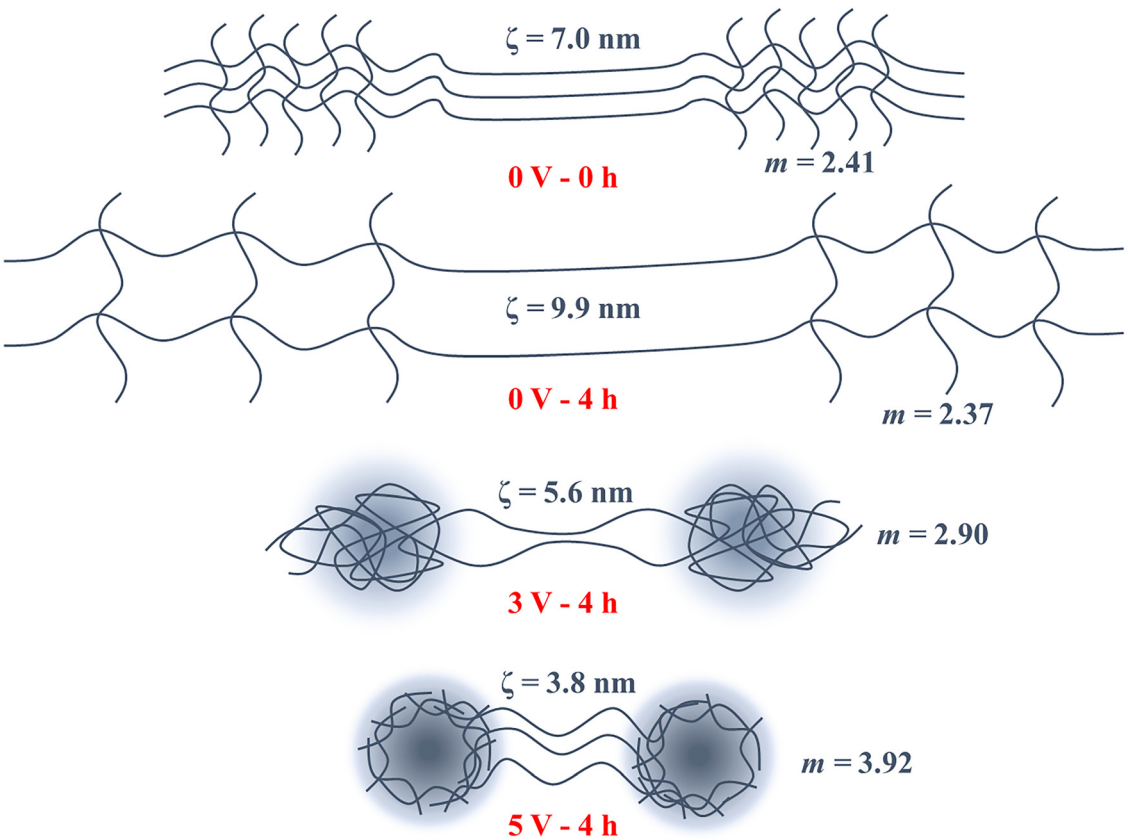

Fig. 8 Scheme of the evolution of the PVA-BA-QCSPA hydrogel network structure model.

and 15.1 nm, respectively. These values are in good general agreement with the values derived from the correlation length model, especially as one has to consider here that they arise from completely different approaches to estimate an effective characteristic length. However, their relative changes upon application of electric field are not consistent, indicating that the reduction of elastic properties cannot be attributed only to average structural changes, but here some additional mechanism that reduces the effective network connectivity must be active.

In summary, swelling in the absence of an electric field just led to a gradually stretched network structure composed of more dilute local domains. In contrast, the observed changes in the fit parameters suggest that electrical stimulation induced a local compaction of the polymer network, with a pronounced structural densification at higher voltage. This behaviour is likely to be attributed to an alignment and reconfiguration of PANI chains under the electric field, resulting in a denser microscopic network. At low voltage, the network underwent slow compaction and mild aggregation, while the higher voltage significantly induced the rearrangement and aggregation of PANI segments, driving a transition of local domains from mass fractal to surface fractal structures and resulting in the formation of a dense conductive structural framework.

3.2.3 Gaussian spherical domain (GSD) fitting. From the single broad peak seen in the Kratky plots (Fig. 5) one may conclude that the hydrogel network contains domains. Within a further analysis of the scattering data these domains were described as spherical structures with a diffuse scattering length density (SLD) profile, approximated by a spherically symmetric Gaussian profile,[45,46] as it should be formed by more or less compacted polymer chains through crosslinking or entanglement. Details of this simple model are given in the SI and the scattering intensity as a function of the sphere radius is therefore obtained as:

$$I(q) = I_2 \cdot \left(R^3 \cdot \mathrm{e}^{\left(-\frac{q^2R^2}{2}\right)} \right)^2 \quad (3)$$

where $I_2 = N(2\pi)^3{\rho_0}^2$, with N being the number density of these aggregates and ρ_0 the SLD at the centre. In order to account for the remaining gel network behaviour a power-law function (I_1/q^n) was added, which then yields for the intensity of the GSD model:

$$I(q) = \frac{I_1}{q^n} + I_2 \cdot \left(R^3 \cdot \mathrm{e}^{\left(-\frac{q^2R^2}{2}\right)} \right)^2 \quad (4)$$

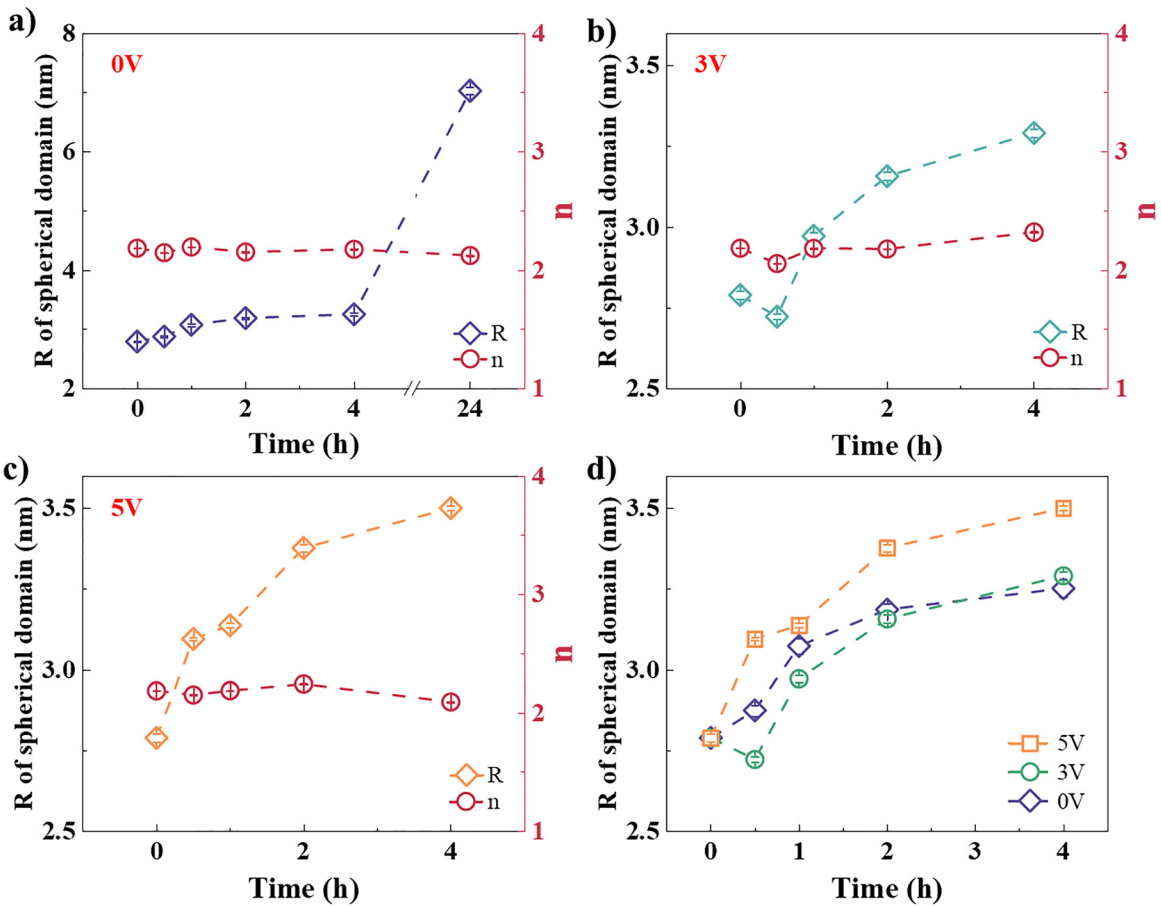

Fig. 9 Fitting parameters (R and n) obtained from the spherical domain model of the PVA-BA-QCSPA hydrogel with the application of (a) 0 V, (b) 3 V, and (c) 5 V. (d) Comparison of GSD R at different voltages over time.

It should be noted that the exponent n in eqn (4) does not correspond to the n from the correlation length model (eqn (2)), as eqn (4) was only applied to describe the region of the peak seen in the Kratky plots (Fig. 5). Accordingly, n from eqn (4) then basically just accounts to describe the background scattering of the overall structure in the size range of 10–50 nm.

Similarly, the high-q region *Bkg* was accounted for in the fitting procedure. The fits in the Kratky peak region, where the scattering is dominated by the local density correlations of the polymer network, yielded as most interesting parameter the effective radius R. The Kratky plots fitted with the GSD model are shown in Fig. 5 (dashed curves), while the corresponding plots at each voltage are presented separately in Fig. S7–S9. The corresponding fitted parameter values are listed in Tables S1, S2, and S3 for the respective voltage conditions of 0 V, 3 V, and 5 V. The most important fitting parameters R and n are presented in Fig. 9. Without applied voltage, as illustrated in Fig. 9a, the radius R of the GSD increased monotonically during 24 hours of swelling in 0.01 M PBS, rising significantly from an initial value of 2.79 nm to 7.03 nm. This reflects continuous swelling, expansion, and loosening of the hydrogel network in the absence of an electric field. Meanwhile, the n value remained stable within the range of 2.12 to 2.20, showing no significant variation, indicating that the overall gel network structure maintained a random coil conformation.

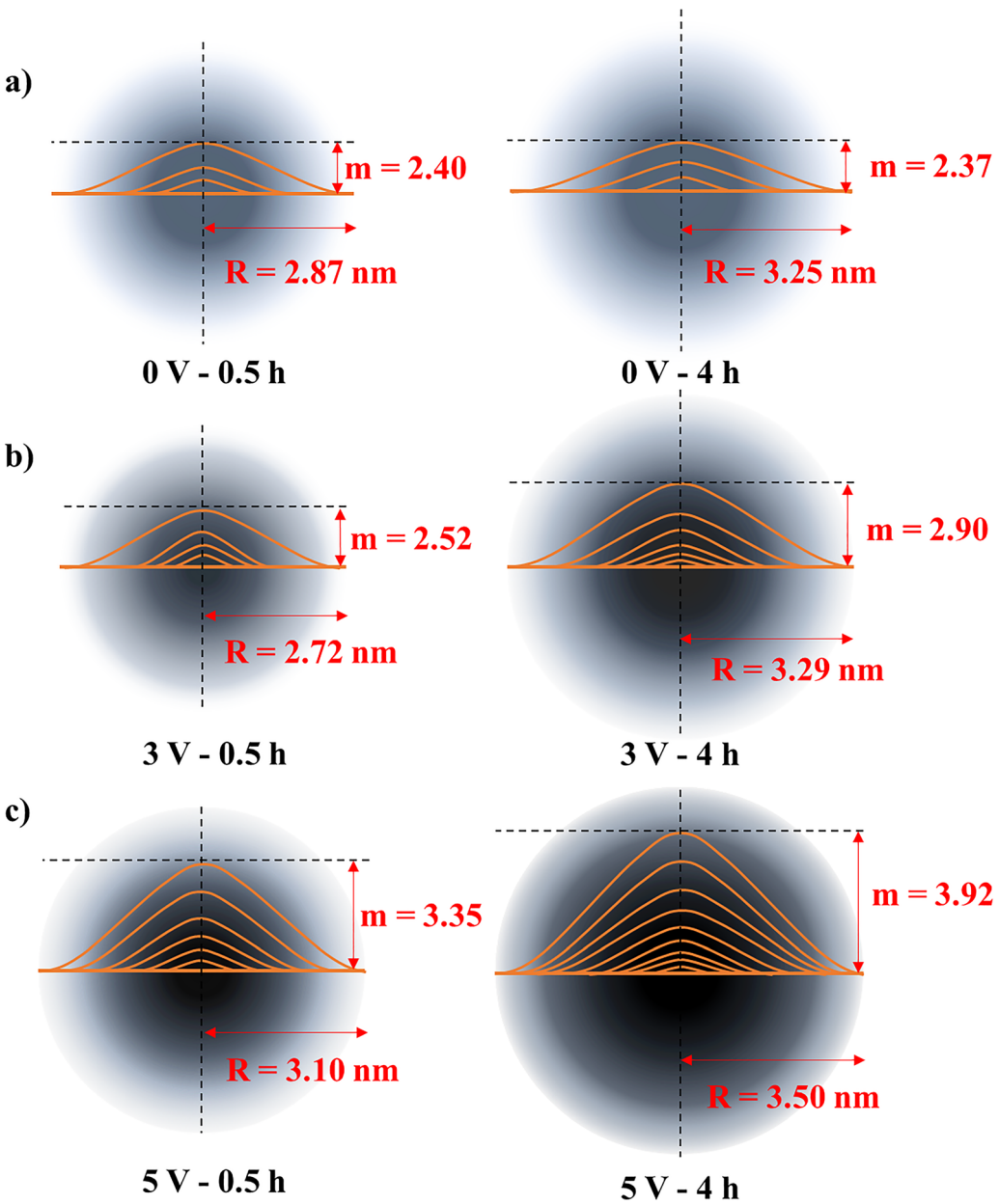

Fig. 10 Schematic diagram of Porod exponent m (from Fig. 7d) and GSD R (from Fig. 9d) varying with voltage and time. The orange line density represents the degree of aggregation, with the colour gradient indicating the Gaussian spherical density distribution.

Upon application of 3 V, as shown in Fig. 9b, the radius R initially decreased slightly at the early stage (0.5 h), then gradually increased, reaching 3.29 nm at 4 hours. This suggests that the electric field initially suppressed network swelling to some extent, promoting chain segment rearrangement and local densification, which caused contraction of the spherical domains and R reduction. However, as the duration of the electric field increased, the degree of chain aggregation rose, and the densified area gradually expanded, causing the domain radius R to progressively increase.

Upon application of 5 V, as shown in Fig. 9c, the radius R of the GSD rapidly increased and continued to grow under the high electric field. This likely results from the stronger field inducing more pronounced orientation and rearrangement of polymer chains, thereby accelerating formation of larger dense regions and causing R to increase more quickly than under 3 V.

The changes in the GSD radius R under different voltages are directly compared in Fig. 9d. All three conditions (0 V, 3 V, and 5 V) exhibit an overall increasing trend, as both continuous swelling and electric field stimulation lead to an increasing GSD radius. However, the underlying mechanisms differ: under swelling conditions (0 V), water molecules permeate the network, increasing the spacing between polymer chains and causing domain expansion that forms a large-scale, loose network structure. At 5 V, the high voltage dominates, likely inducing stronger orientation, rearrangement, and aggregation of PANI chains, resulting in the formation of larger domains. At 3 V, the combined regulation of electric field forces and swelling is more evident. The polymer chains undergo local rearrangement and densification under the electric field, initially suppressing swelling-induced expansion, which causes R to temporarily decrease. Over time, in addition to swelling-driven growth, continued aggregation and clustering of polymer chains under the electric field contribute to a further increase in domain size.

Based on the changes in the exponent m from the correlation length model (Fig. 7d) and the effective radius R from the GSD model (Fig. 9d), a schematic diagram illustrating the domain evolution under different electric fields is presented in Fig. 10. During natural swelling, the domain size increases while maintaining a mass fractal character. With increasing voltage and prolonged application time, m rises from 2.40 to 3.92, indicating a gradual transition of domains from mass fractal to surface fractal structures. Meanwhile, the domain radius R initially decreases slightly before continuously increasing, suggesting that the electric field effect begins with local contraction and aggregation, followed by growth and densification. Therefore, at 5 V/4 h, the spherical domain exhibits the largest radius and highest degree of aggregation, and is closer to a smooth surface with a sharp interface.

Overall, the electric field influences domain behaviour in two aspects: it suppresses the uniform expansion and loosening caused by swelling, while simultaneously promoting continuous chain segment rearrangement and restructuring, leading to densification, aggregation, and expansion of the domains. Mechanistically, this field response arises from a coupled multiscale process. At the material level, the DC electric field interacts primarily with the conductive QCSPA phase, driving ion migration and electro-osmotic transport in PBS and thereby accelerating water uptake. At the network level, the resulting ionic redistribution and local changes in concentration/pH promote dissociation of the dynamic boronate crosslinks and weaken hydrogen bonding and ionic interactions, which reduces the effective network connectivity and facilitates rapid rearrangement. At the domain level, multiple pieces of evidence, including a Kratky peak shift to high-q, a decrease in the correlation length ξ, an increase in the exponent m, and an increase in the GSD R, consistently point to field-induced nanoscale densification, leading to a transition in the fractal structure, enhanced structural heterogeneity, and the aggregation and rearrangement of chain-segments. This reveals a synergistic regulatory mechanism between electric field stimulation and swelling on the microstructure of the PVA-BA-QCSPA conductive hydrogel, where the electric field enhances densification and aggregation, swelling drives overall network expansion, and their interplay shapes the dynamic evolution of multiscale structures.

4. Conclusion

This study systematically investigated the microstructural mechanism and evolution of a PVA-BA-QCSPA conductive hydrogel under varying DC electric fields. The hydrogel network was primarily constructed *via* dynamic boronate ester crosslinks. QCSPA is incorporated as a conductive polymer component and participates in the interaction, such as hydrogen bonding, entanglement, and electrostatic interactions.

In this work we studied in detail the rheological properties and the mesoscopic structure, by *in situ* SAXS experiments as a function of an applied voltage. Macroscopically, both the storage modulus and loss modulus decreased with increasing voltage and duration of electric field application. Especially under a high electric field, the network elasticity loss was significant, and the hydrogel suffered the highest degree of softening accompanied by erosion-like mass loss, indicating that the electric field can effectively modify the mechanical properties of the hydrogel. Consistent with the swelling behaviour, these results suggest that electrical stimulation can accelerate network weakening, particularly at higher voltage and longer times. Mechanistically, the electric field couples most strongly to the conductive QCSPA phase, driving ion migration and electro-osmotic transport that generates local concentration gradients. In addition, field-induced ionic redistribution (and potentially local Joule heating and pH variations) can indirectly promote the dissociation of boronate ester crosslinks and weaken interactions, thereby reducing the effective crosslink density and facilitating network rearrangement.

For gaining insights into the mesoscopic structure of the hydrogel under the electric field and swelling by water, the SAXS data on samples exposed to a certain voltage and for different times were obtained. The correlation length model

uncovered a microstructural evolution of the hydrogel network under applied electric field—from an initially loose, random coil structure toward a more compacted fractal organization. Particularly at high voltage, the local domains gradually transformed from a mass fractal to a surface fractal, accompanied by enhanced densification of the network. The Gaussian spherical domain fitting revealed the growth and evolution process of spherical domains of 3–5 nm radius. The electric field can significantly suppress domain swelling in the initial stage, promote chain densification and local rearrangement, and cause the Gaussian domain size initially to decrease and then increase again, reflecting the competitive effect between swelling-driven expansion and electric field-driven densification. Under stronger electric fields, larger and more dense domains are formed more rapidly. These structural changes correlate with the accelerated decreases in G' and G'' and the erosion-like mass loss, thus linking microstructural evolution to the macroscopic weakening of the hydrogel.

Overall, this investigation into the effect of electric field under swelling conditions on a PVA-BA-QCSPA conductive hydrogel provides substantial insights into their behaviour, which is central to their use in electro-driven drug delivery and other electrically responsive applications. In particular, it becomes clear that for a longer-lasting use of this system not too high voltages should be applied. In future work, this foundation enables further performance optimization through systematic composition-property tuning, and facilitates the development of improved electro-responsive hydrogels with optimized molecular composition.

Author contributions

L. T.: conceptualization, data curation, formal analysis, investigation, methodology, validation, visualization, writing – original draft. Y. S.: conceptualization, investigation, methodology, software, validation. R. F. S.: software. C. B.: investigation, resources, data curation. M. G.: funding acquisition, project administration, resources, supervision, writing – review & editing.

Conflicts of interest

There are no conflicts to declare.

Data availability

The data supporting this article have been included as part of the supplementary information (SI). Supplementary information is available. See DOI: https://doi.org/10.1039/d6tb00211k.

Acknowledgements

This study and the authors acknowledge the Deutsche Forschungsgemeinschaft (DFG, German Research Foundation) – SFB 1449-431232613 project A02 for financial support. L. T. and Y. S. acknowledge the China Scholarship Council (CSC) for financial support. R. F. S. would like to acknowledge the Fonds der Chemischen Industrie (FCI) for financial support. Further, we thank Jana Lutzki and Michaela Dzionara for substantial contributions on the experimental preparation and configuration. We gratefully acknowledge the EMBL Hamburg (European Molecular Biology Laboratory, Hamburg Outstation) for granting beamtime (experiment number SAXS-1316, beamline P12).

References

1 E. M. Ahmed, *J. Adv. Res.*, 2015, **6**, 105–121.
2 T. C. Ho, C. C. Chang, H. P. Chan, T. W. Chung, C. W. Shu, K. P. Chuang, T. H. Duh, M. H. Yang and Y. C. Tyan, *Molecules*, 2022, **27**, 2902.
3 F. Andrade, M. M. Roca-Melendres, E. F. Duran-Lara, D. Rafael and S. Schwartz, Jr., *Cancers*, 2021, **13**, 1164.
4 Z. Yang, L. Chen, D. J. McClements, C. Qiu, C. Li, Z. Zhang, M. Miao, Y. Tian, K. Zhu and Z. Jin, *Food Hydrocolloids*, 2021, **124**, 107218.
5 S. J. Jeon, A. W. Hauser and R. C. Hayward, *Acc. Chem. Res.*, 2017, **50**, 161–169.
6 N. Sood, A. Bhardwaj, S. Mehta and A. Mehta, *Drug Delivery*, 2016, **23**, 758–780.
7 Q. Shi, H. Liu, D. Tang, Y. Li, X. Li and F. Xu, *NPG Asia Mater.*, 2019, **11**, 64.
8 Z. Deng, R. Yu and B. Guo, *Mater. Chem. Front.*, 2021, **5**, 2092–2123.
9 R. D. Pyarasani, T. Jayaramudu and A. John, *J. Mater. Sci.*, 2019, **54**, 974–996.
10 T. Zhu, Y. Ni, G. M. Biesold, Y. Cheng, M. Ge, H. Li, J. Huang, Z. Lin and Y. Lai, *Chem. Soc. Rev.*, 2023, **52**, 473–509.
11 L. Wang, T. Xu and X. Zhang, *TrAC, Trends Anal. Chem.*, 2021, **134**, 116130.
12 M. Beygisangchin, A. Hossein Baghdadi, S. Kartom Kamarudin, S. Abdul Rashid, J. Jakmunee and N. Shaari, *Eur. Polym. J.*, 2024, **210**, 112948.
13 P. Humpolicek, V. Kasparkova, J. Pachernik, J. Stejskal, P. Bober, Z. Capakova, K. A. Radaszkiewicz, I. Junkar and M. Lehocky, *Mater. Sci. Eng., C*, 2018, **91**, 303–310.
14 N. Sharma, A. Singh, N. Kumar, A. Tiwari, M. Lal and S. Arya, *J. Mater. Sci.*, 2024, **59**, 6206–6244.
15 M. Beygisangchin, S. Abdul Rashid, S. Shafie, A. R. Sadrolhosseini and H. N. Lim, *Polymers*, 2021, **13**, 2003.
16 E. N. Zare, P. Makvandi, B. Ashtari, F. Rossi, A. Motahari and G. Perale, *J. Med. Chem.*, 2020, **63**, 1–22.
17 X. Zhao, H. Wu, B. Guo, R. Dong, Y. Qiu and P. X. Ma, *Biomaterials*, 2017, **122**, 34–47.
18 X. Zhao, P. Li, B. Guo and P. X. Ma, *Acta Biomater.*, 2015, **26**, 236–248.
19 M. Shibayama, *Soft Matter*, 2012, **8**, 8030–8038.
20 S. S. Welborn and E. Detsi, *Nanoscale Horiz.*, 2020, **5**, 12–24.
21 C. M. Jeffries, M. A. Graewert, C. E. Blanchet, D. B. Langley, A. E. Whitten and D. I. Svergun, *Nat. Protoc.*, 2016, **11**, 2122–2153.

22 G. Polymeropoulos, G. Zapsas, K. Ntetsikas, P. Bilalis, Y. Gnanou and N. Hadjichristidis, *Macromolecules*, 2017, **50**, 1253–1290.
23 D. J. Waters, K. Engberg, R. Parke-Houben, L. Hartmann, C. N. Ta, M. F. Toney and C. W. Frank, *Macromolecules*, 2010, **43**, 6861–6870.
24 S. L. Pesek, X. Li, B. Hammouda, K. Hong and R. Verduzco, *Macromolecules*, 2013, **46**, 6998–7005.
25 Y. Wei and M. J. A. Hore, *J. Appl. Phys.*, 2021, **129**, 171101.
26 E. M. Saffer, M. A. Lackey, D. M. Griffin, S. Kishore, G. N. Tew and S. R. Bhatia, *Soft Matter*, 2014, **10**, 1905–1916.
27 C. Hotton, G. Ducouret, J. Sirieix-Plénet, T. Bizien, L. Porcar and N. Malikova, *Macromolecules*, 2023, **56**, 923–933.
28 L. L. E. Mears, E. R. Draper, A. M. Castilla, H. Su, Z. Zhuola, B. Dietrich, M. C. Nolan, G. N. Smith, J. Doutch, S. Rogers, R. Akhtar, H. Cui and D. J. Adams, *Biomacromolecules*, 2017, **18**, 3531–3540.
29 S. Wang, C. Jiao, G. Gerlach and J. Korner, *Biomacromolecules*, 2024, **25**, 2715–2727.
30 J. Cho, J. Grant, M. Piquette-Miller and C. Allen, *Biomacromolecules*, 2006, **7**, 2845–2855.
31 C. Luo, H. Peng, L. Zhang, G.-L. Lu, Y. Wang and J. Travas-Sejdic, *Macromolecules*, 2011, **44**, 6899–6907.
32 A. M. Omer, Z. M. Ziora, T. M. Tamer, R. E. Khalifa, M. A. Hassan, M. S. Mohy-Eldin and M. A. T. Blaskovich, *Molecules*, 2021, **26**, 449.
33 L. Boldon, F. Laliberte and L. Liu, *Nano Rev.*, 2015, **6**, 25661.
34 D. Liu, K. Song, W. Chen, J. Chen, G. Sun and L. Li, *Nucl. Anal.*, 2022, **1**, 100011.
35 P. Malo de Molina, D. Kafouris, C. S. Patrickios, L. Noirez and M. Gradzielski, *Macromolecules*, 2023, **56**, 8323–8332.
36 C. D. Putnam, M. Hammel, G. L. Hura and J. A. Tainer, *Q. Rev. Biophys.*, 2007, **40**, 191–285.
37 P. Bernado and D. I. Svergun, *Mol. BioSyst.*, 2012, **8**, 151–167.
38 V. M. Burger, D. J. Arenas and C. M. Stultz, *Sci. Rep.*, 2016, **6**, 29040.
39 Y. Shinohara, K. Kayashima, Y. Okumura, C. Zhao, K. Ito and Y. Amemiya, *Macromolecules*, 2006, **39**, 7386–7391.
40 R. P. Rambo and J. A. Tainer, *Biopolymers*, 2011, **95**, 559–571.
41 B. Hammouda, D. L. Ho and S. Kline, *Macromolecules*, 2004, **37**, 6932–6937.
42 G. Porod, *Kolloid-Z.*, 1951, **124**, 83–114.
43 W. L. Tan, L. Tang, R. Matsidik, G. Bryant, T. B. Martin, M. Sommer, D. M. Huang and C. R. McNeill, *Macromolecules*, 2024, **57**, 691–706.
44 G. Yuan, X. Wang, D. Wu and B. Hammouda, *Polymer*, 2016, **100**, 119–125.
45 Y. Kamijo, K. Fujimoto, H. Kawaguchi, Y. Yuguchi, H. Urakawa and K. Kajiwara, *Polym. J.*, 1996, **28**, 309–316.
46 C. M. Jeffries, J. Ilavsky, A. Martel, S. Hinrichs, A. Meyer, J. S. Pedersen, A. V. Sokolova and D. I. Svergun, *Nat. Rev. Methods Primers*, 2021, **1**, 70.